Surface & Coatings Technology 253 (2014) 109–114

Contents lists available at ScienceDirect

Surface & Coatings Technology

journal homepage: www.elsevier.com/locate/surfcoat

Relationship between film composition and microhardness of electrodeposited Ni–W–B films prepared using a citrate–glycinate bath

Taichi Nagai, Kazunori Hodouchi, Hiroshi Matsubara *

Department of Materials Science and Technology, Nagaoka University of Technology, 1603-1 Kamitomioka, Nagaoka 940-2188, Japan

ARTICLE INFO

Article history:
Received 3 December 2013
Accepted in revised form 10 May 2014
Available online 24 May 2014

Keywords:
Ni–W–B alloy film
Electrodeposition
Dimethylamine borane
Microhardness
Microstructure

ABSTRACT

In the present study, the authors fabricated the electrodeposited Ni–W–B films with various W and B contents and evaluated their composition, surface morphology, crystal structure and microhardness. The Ni–W–B films were deposited using a Ni–W plating bath containing dimethylamine borane as the boron source and citrate and glycine as complexing agents. It was possible to prepare Ni–W–B films with a wide range of W (0–19 at.%) and B (0–18 at.%) content by controlling the plating condition (tungstate concentration, glycine concentration and current density). The hardness of the Ni–W–B films with a nanocrystalline phase was proportional to the square root of the grain size, in accordance with the Hall–Petch relation. However, in the region of amorphous or nanocrystalline phase of 2–3 nm or less in grain size, hardness decreased. The maximum hardness of the Ni–W–B films was about 850 Hv, comparable to that of hard chromium plated films. It is very important to optimize the film composition in order to fabricate Ni–W–B films with high hardness.

1. Introduction

Chromium plating is applied to a wide range of industrial fields because of its advantageous properties such as wear resistance, high hardness and esthetic appearance.

However, since hexavalent chromium, which is present in the plating solution, is toxic to the environment and human health, an alternative technology is required.

As a possible alternative, Ni–W–B electroplating films have been developed. Ni–W–B films can be electrodeposited from an Ni–W electrolyte solution containing a boric compound such as borate [1–5], dimethylamine borane [6,7], a borohydride [8] or boron phosphate [9,10].

Several papers have reported on the hardness of as-deposited Ni–W–B films. For example, Hosseini et al. reported that the $Ni_{81.8}W_{7.4}B_{10.8}$ (at.%) film had a hardness of around 600–850 Hv [4]. Moreover, they reported a maximum hardness of 875 Hv for $Ni_{72.4}W_{15.2}B_{12.4}$ (at.%) film electrodeposited using a tartrate bath with 2-butyne-1,4-diol as a brightener [5]. Employing a citrate ammoniacal bath, Yang et al. demonstrated that electrodeposited $Ni_{81.1}W_{12.4}B_{6.6}$ (at.%) film had a hardness of 612 Hv [7]. Graef et al. reported that $Ni_{81.6}W_{11.9}B_{6.5}$ (at.%) film had a hardness of 600 Hv [11] and Croopnick reported that $Ni_{76.7}W_{16.3}B_{7.0}$ (at.%) film had a hardness of 600 Hv [12], although details of the plating conditions used in these studies are unknown.

Thus, as seen from the above, studies on the hardness of Ni–W–B plating film compositions are rather limited and there are no conclusive reports on the relationship between hardness and film composition.

Traditional Ni–W plating baths contain ammonia and citrate as complexing agents. Ammonia contributes to improve current efficiency. However, it also reduces the bath stability and has problems for the work environment due to its volatility. Wu et al. investigated the use of glycine as an alternative to ammonia in the Ni–W citrate bath and found that glycinate reduced the W content in the film and improved current efficiency [13].

In this study, we used a Ni–W plating bath containing citrate and glycine as complexing agents and dimethylamine borane (DMAB) as the boron source. We examined the effective plating conditions to co-deposit boron with the Ni–W film. We also attempted to fabricate Ni–W–B plated films with a wide range of W and B content. The purpose of this study was to clarify the effects of film composition on the microhardness of ternary Ni–W–B alloy plated films with a wide range of composition.

2. Experimental

The plating bath compositions and operating conditions used in this study are listed in Table 1. The Ni–W–B films were prepared using baths (I)–(IV) and the Ni–W films were prepared from bath (V). The metal sources used were nickel sulfate and sodium tungstate. DMAB was added to the bath to provide boron. Sodium citrate and glycine were added as complexing agents. Pure Ni film was electrodeposited from an additive-free Watts bath ($NiSO_4$ 1.07 mol dm^{-3}, $NiCl_2$

* Corresponding author. Tel./fax: +81 258 47 9834.
E-mail address: maruma@analysis.nagaokaut.ac.jp (H. Matsubara).

http://dx.doi.org/10.1016/j.surfcoat.2014.05.022
0257-8972/

Table 1
Bath compositions and operating conditions used for the Ni–W and Ni–W–B films.

Concentration (mol dm^{-3})					
	(I)	(II)	(III)	(IV)	(V)
Nickel sulfate($NiSO_4 \cdot 6H_2O$)	0.10	0.10	0.10	0.10	0.10
Sodium tungstate ($Na_2WO_4 \cdot 2H_2O$)	0.10	0.05	0.15	0.20	0.20
Dimethylamine borane ($(CH_3)_2NHBH_3$)	0.10	0.10	0.10	0.10	–
Sodium citrate ($Na_3C_6H_5O_7 \cdot 2H_2O$)	0.40	0.40	0.40	0.40	0.40
Glycine (NH_2CH_2COOH)	0.01–0.40	0.01–0.20	0.01–0.20	0.01–0.20	0.01–0.40
pH (H_2SO_4/NaOH)	7	7	7	7	7
Temperature/K	323	323	323	323	323
Agitation speed/rpm	250	250	250	250	250
Current density/A dm^{-2}	0.5–5.0	0.5–2.0	0.5–2.0	0.5–2.0	1.0

0.19 mol dm^{-3}, H_3BO_3 0.65 mol dm^{-3}, 3.0 A dm^{-2}, using Ni plate as anode) for comparison.

A platinum plate (30 mm × 40 mm) was used as an insoluble anode and a copper plate (20 mm × 100 mm) was used as the cathode. Prior to the electrodeposition, the cathode substrate was polished mechanically to a mirror finish with an Al_2O_3 slurry (1 μmφ). The plating area was limited to 20 mm × 20 mm by masking with insulating tape. The substrate was ultrasonically cleaned in an ethanol solution for 3 min, etched in 50% HCl solution for 2 min and then washed with distilled water. The distance between the anode and cathode was 10 mm, and they were arranged in parallel.

All the experiments were carried out at 323 K and at a bath pH of 7, the bath volume was 100 cm^3, and the stirring rate was 250 rpm using a magnetic stirrer. The film thickness was adjusted to 5 ± 0.5 μm. Nickel complexes in the plating solutions were analyzed by means of UV–Vis spectrum analysis (V-570, JASCO). The deposition rate and composition of the plated film were measured by glow discharge optical emission spectrometry (GD-OES, GD-Profiler 2, HORIBA). Anodic polarization measurements were performed in a cell consisting of a three-electrode system using an electrochemical measurement system (HZ3000, HOKUTO DENKO). A Cu plate (measurement area 20 mm × 20 mm) was used as the working electrode. An Ag/AgCl electrode and a Pt plate (30 mm × 40 mm) were used as the reference and counter electrodes, respectively. The scanning rate of the electrode potential was 5 mV s^{-1}. The microstructure was observed using a scanning electron microscope (JSM-6010LA, JEOL, 15 kV). The microhardness was measured by a nanoindenter (PICODENTOR HM500, FISCHER), with 15 mN loading. Each hardness value was determined by averaging five measurements. Structural analysis was performed by means of X-ray diffraction (RINT-2200HF$^+$/PC, RIGAKU) using Cu Kα radiation at 40 kV and 30 mA. The grain size was estimated from the half-width of the (111) diffraction peak according to the Scherrer formula. For the XRD measurements, films with thickness greater than 15 μm were prepared in order to reduce the influence of the peak from the Cu substrate.

3. Results and discussion

3.1. Preparation of ternary Ni–W–B alloy films

3.1.1. UV–Vis spectra of the electrolyte

UV–Vis measurements were conducted to identify each complex in the plating solution. UV–Vis spectra of bath (I) with various glycine concentrations are shown in Fig. 1. Two peaks observed for the glycine free solution were identified to be ternary complexes of the type $[(Ni)(HWO_4)(Cit)]^{2-}$ [14]. The two peaks shifted to shorter wavelengths by the addition of glycine, and approached the absorption wavelength of the citrate free Ni-glycinate-tungstate complex [15]. It is suggested that the proportion of the glycinate complex increased with increasing glycine concentration.

3.1.2. Deposition rate and film composition

Fig. 2 shows the effect of the current density on the deposition rate (a), W content in the film (b) and B content in the film (c) when using bath (I) with various glycine concentrations. The deposition rate increased with an increasing current density and increasing concentration of glycine. Wu et al. reported that glycine was effective in increasing the deposition efficiency in Ni–W electrodeposition [13]. A similar tendency was observed in this study. The film composition depended on the plating current density and the glycine concentration. As the plating current density increased, the W and B contents of the plated film decreased. On the other hand, the W content of the film decreased and the B content of the film increased when the glycine concentration was increased. Younes and Gileadi reported that the precursor for the W deposition is a ternary complex of $[(Ni)(HWO_4)(Cit)]^{2-}$ [14]. On the other hand, it has been reported that the Ni-glycinate complex formed in this study is directly reduced to the deposit [13]. The Ni-glycine complex formation decreases the amount of the precursor $[(Ni)(HWO_4)(Cit)]^{2-}$ complex for W deposition. Thus, the W content of the film is considered to decrease with increasing glycine concentration.

3.1.3. Mechanism of B co-deposition

A higher B content in the film is observed for a lower plating current density, as seen in Fig. 2(c). In this study, we employed DMAB as the B source, which is well known as a reducing agent. Cao et al. [6] have reported that the electrodeposition of Ni–W–B films from an electrolyte containing DMAB can be accompanied by an electroless deposition reaction. Based on previous reports, it is expected that there is some relationship between the oxidation reaction of DMAB and the B content of the deposited film. Therefore, we conducted anodic polarization

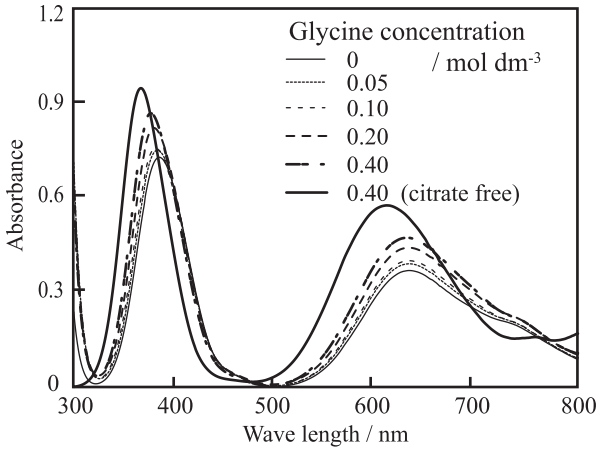

Fig. 1. UV–Vis spectra of bath (I) solutions with various glycine concentrations.

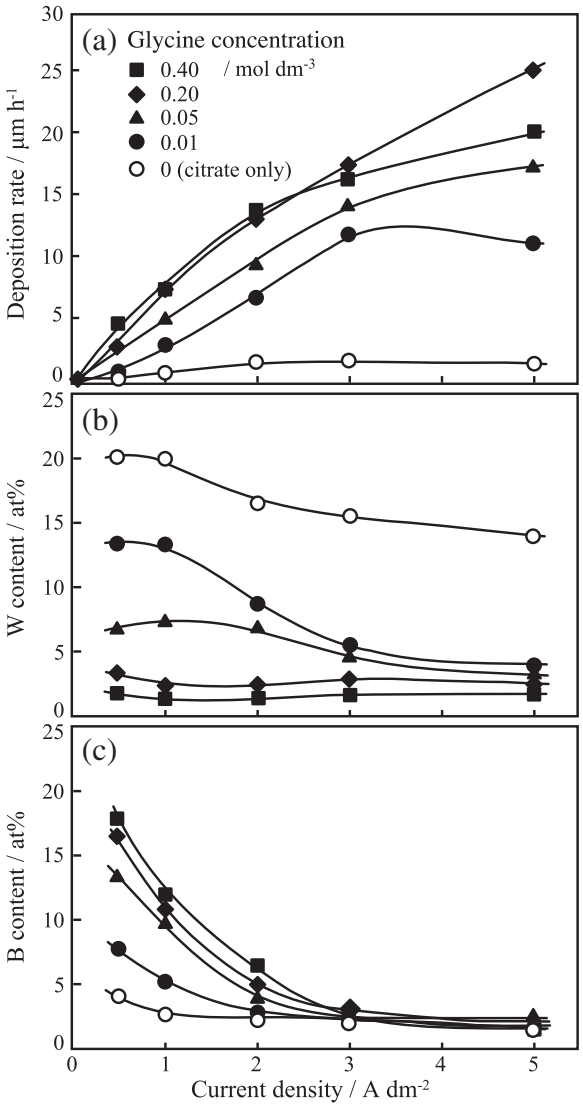

Fig. 2. The effect of current density on the deposition rate (a), W content (b), and B content (c) of the films deposited from bath (I).

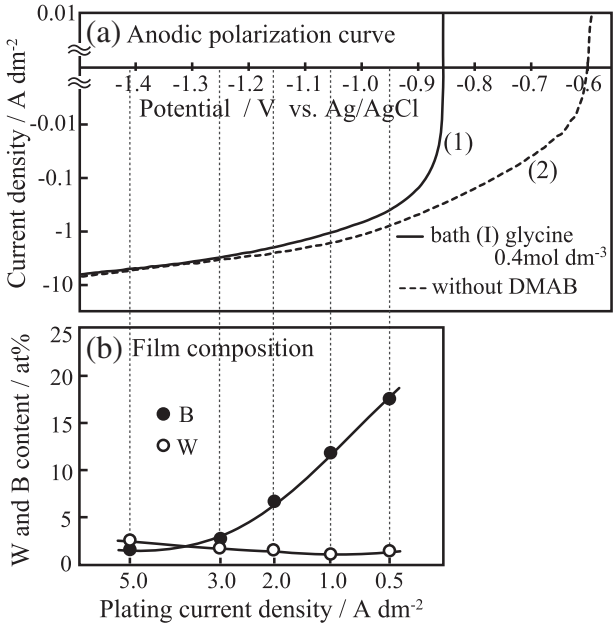

Fig. 3. Relationship between deposition potential and film composition.

measurements in bath (I) (glycine 0.4 mol dm^{-3}) as well as in the bath without DMAB. The results of the anodic polarization measurement are shown in Fig. 3(a) associated with the relationship between the plating current density and the film composition Fig. 3(b). In Fig. 3(b) the current density is plotted in correspondence to the potential which is plotted in Fig. 3(a). We find, in the anodic scan shown in Fig. 3(a), that the cathodic current density plotted as a solid line (curve1) became smaller than that potted as a dashed line (curve2) over ca. −1.25 V. The difference between curve 1 and curve 2 is caused by the presence of DMAB. Oxidation of DMAB is indicated at a potential around −1.25 V in curve 1 and then accelerates according to the anodic scan. This results in a decrease in the current density. Fig. 3(b) shows that when the plating current density was lower than 3 A dm^{-2}, the B content of the film increased. The plating current density of 3 A dm^{-2} corresponds to a potential of −1.25 V in this plating condition. That is, co-deposition of B in the plating film takes place at a potential nobler than the oxidation potential of DMAB.

3.1.4. Preparation of Ni–W–B films with various compositions

We fabricated Ni–W–B films using baths with different W concentrations, as shown in Table 1 (baths (II)–(IV)), in order to prepare Ni–W–B plated films with various W and B contents. Electroplating was performed at a low current density (0.5–2 A dm^{-2}) for effective co-deposition of B in the film. Ni–W and pure Ni films were also prepared using bath (V) and a Watts bath, respectively.

The results are summarized in Fig. 4. As shown in the figure, it was possible to prepare ternary Ni–W–B alloy films with a wide range of W (0–19 at.%) and B (0–18 at.%) content by controlling the plating conditions used (including tungstate and glycine concentrations and the plating current density).

3.2. Characterization of Ni–W–B films

3.2.1. Surface morphology

A few cracks were found in each Ni–W–B plated film. However, no cracks were observed in most of the surface. Fig. 5 shows typical surface morphology of the Ni–W–B films. Although small nodules were

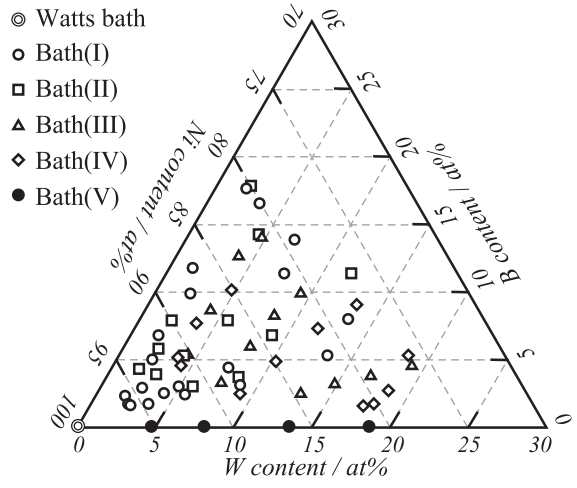

Fig. 4. Composition of ternary Ni–W–B alloy films deposited from baths (I)–(V).

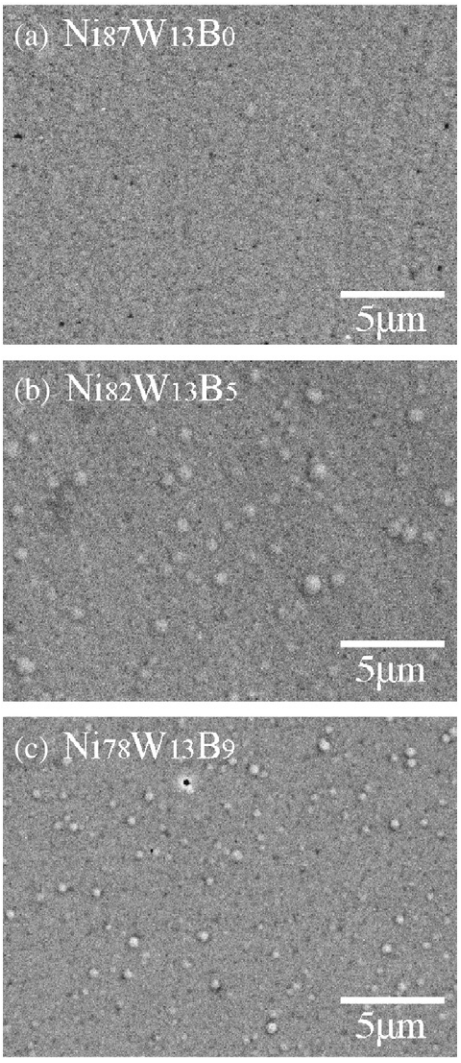

Fig. 5. Surface morphology of ternary Ni–W–B alloy films deposited from (a) bath (V) (glycine 0.05 mol dm^{-3}, 1.0 A dm^{-2}) (b) bath (I) (glycine 0.0 mol dm^{-3}, 1.0 A dm^{-2}) (c) bath (IV) (glycine 0.05 mol dm^{-3}, and 0.5 A dm^{-2}).

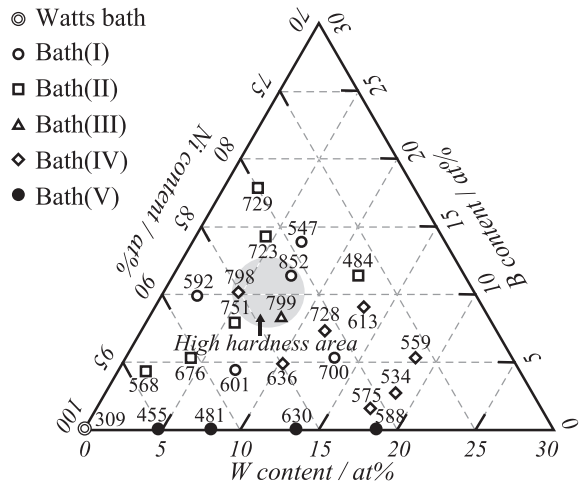

Fig. 6. Relationship between microhardness and composition of ternary Ni–W–B alloy films.

observed in Fig. 5(b) (c), a relatively smooth surface was found in most of the films which have varying compositions.

3.2.2. Relationship between microhardness and film composition

The hardness values of the typical films shown in Fig. 4 are indicated in Fig. 6. The hardness of the electrodeposited pure Ni film from an additive-free Watts bath was 309 Hv. The hardness of the Ni–W–B films prepared in this study ranged from 500 to 850 Hv, higher than that of the conventional pure Ni film. The region with the highest hardness was $Ni_{82-86}W_{4-8}B_{8-12}$ (at.%). The composition of the Ni–W–B films in the area is shown with gray color in Fig. 6. The hardness of the films in this region was ca. 800–850 Hv, comparable to that of hard chromium plated films. It is very important to optimize the film composition in order to fabricate Ni–W–B films with high hardness.

3.2.3. X-ray diffraction analysis

The X-ray diffraction patterns of the typical films shown in Fig. 4 are indicated in Fig. 7. Diffraction patterns (a), (d) and (g) in Fig. 7 are those of Ni–W plated films with different W contents. The peak intensity decreased and the peak width broadened with increasing W content. Also, the Ni(W)(111) peak (43.50 deg.) shifted to lower angles, compared to pure nickel (44.49 deg.) because the dissolution of W atoms in nickel led to some expansion of the fcc nickel lattice [15]. In Fig. 7(a), it is seen that there is an unknown peak at 41.20 deg. other than the Ni(W)(111) peak. This peak has also been pointed out by other researchers [13, 15–17]. Mizushima et al. reported that this peak is due to anomalous phase co-deposition such as nanocrystalline Ni(–W) or Ni–W–C phases [16]. Juškėnas et al. determined the phase to be nonstoichiometric $NiWO_4$ [17]. This anomalous phase could be eliminated by co-deposition of B or by increasing W content. The peak intensity of Ni(W)(111) decreased and the peak width broadened, by the co-deposition of B in the films with various W contents. The grain size was calculated from the half-width of the (111) diffraction peak by using the Scherrer formula, as shown in Fig. 8.

Although the concept of radial distribution might be necessary for the analysis of diffraction patterns in a nanocrystalline region less than several nm grain sizes, we simply estimated the grain size using the Scherrer formula in this study. The grain size decreased with increasing W content in the Ni–W film. Moreover, the grain size decreased by the co-deposition of boron in the films with various W contents. Refinement of grain size due to co-deposition of W [18–20] or B [21,22] with fcc Ni has been reported. Our results in Fig. 8 are consistent with those in previous reports.

Fig. 9 shows the relationship between the estimated grain size and the film composition of Ni–W–B plated films. It was confirmed that the grain size decreased with increasing W and B contents in all the films which have various compositions, as shown in the figure. It has been reported that both $Ni_{80}W_{20}$(at.%) plated film [18,19] and $Ni_{78}B_{22}$(at.%) plated film [21] have an amorphous structure. Giga et al. [23] performed TEM observations of Ni–W plated film with a grain size of 2 nm estimated from XRD patterns, and they concluded that it was also an amorphous structure. Based on the above reports, a plated film with a grain size of less than 2 nm was considered as an amorphous structure. From the above results, the Ni–W–B films were classified into an amorphous phase or a nanocrystalline phase in Fig. 9. It was found that films with Ni content less than ca. 80 at.% in the Ni–W–B films prepared in this study were amorphous.

3.2.4. Hall–Petch plot of ternary Ni–W–B alloy films

The relationship between hardness (Fig. 6) and grain size (Fig. 9) is shown in Fig. 10. It can be seen that the hardness of the Ni–W–B films is proportional to the square root of the grain size in the nanocrystalline phase; this is almost in accordance with the Hall–Petch relation. Therefore, the hardness increased because the propagation of dislocations

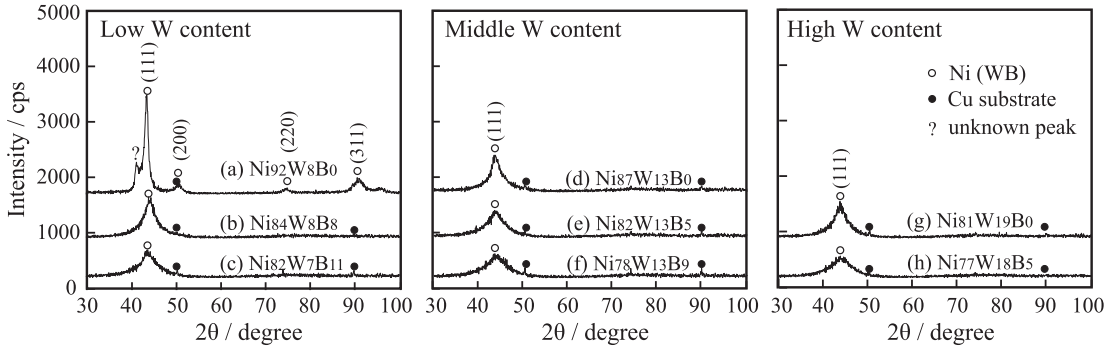

Fig. 7. X-ray diffraction patterns of ternary Ni–W–B alloy films deposited from

(a) bath (V) (glycine 0.20 mol dm^{-3}, 1.0 A dm^{-2})
(b) bath (III) (glycine 0.05 mol dm^{-3}, 1.0 A dm^{-2})
(c) bath (I) (glycine 0.05 mol dm^{-3}, 1.0 A dm^{-2})
(d) bath (V) (glycine 0.05 mol dm^{-3}, 1.0 A dm^{-2})
(e) bath (I) (glycine 0.01 mol dm^{-3}, 1.0 A dm^{-2})
(f) bath (IV) (glycine 0.05 mol dm^{-3}, 0.5 A dm^{-2})
(g) bath (V) (glycine 0.01 mol dm^{-3}, 1.0 A dm^{-2})
(h) bath (IV) (glycine 0.01 mol dm^{-3}, 0.5 A dm^{-2}).

was inhibited by the grain boundary in the nanocrystalline Ni–W–B films.

Plated films with high hardness (800–850 Hv) described above were obtained in the grain size region of 2–3 nm. However, plated films with 2–3 nm grain size did not necessarily have a high hardness. As can be seen in Fig. 6, the high hardness region was $Ni_{82-86}W_{4-8}B_{8-12}$ (at.%). Schuh et al. [24] reported that mechanistic contributions to the strength of nanocrystalline Ni–W films represented a total of solid solution strengthening, grain refinement, and intrinsic hardness of a high-purity single crystal Ni. It is considered that high hardness is achieved by a combination of such factors.

In the grain size region less than 2–3 nm in Fig. 10, the hardness decreased. It is considered that grain boundary sliding dominated the hardness in the region. This phenomenon is the so-called inverse Hall–Petch relationship. However, a detailed mechanism of hardness reduction is currently unknown in such an amorphous-like structure. The hardness reduction according to the inverse Hall–Petch relationship has been reported for less than 14 nm for pure Ni film [25] and less than 8 nm for the binary Ni–W alloy film [24]. It is considered that the region of the hardness reduction shifted to less than 2–3 nm due to ternary alloy formation by the addition of B in the Ni–W film. Since the hardness of the nanocrystalline region of 2–3 nm grain size increased by ternary alloy formation, high hardness of Ni–W–B films was accomplished in this study.

4. Conclusion

In this study, Ni–W–B films were fabricated using a Ni–W plating bath containing dimethylamine borane as a boron source and citrate and glycine as complexing agents.

The results obtained are as follows;

1. Co-deposition of B in the Ni–W film occurs efficiently in the region of low current density of the plating potential nobler than the oxidation potential of DMAB.
2. It was possible to prepare Ni–W–B films with a wide range of W (0–19 at.%) and B (0–18 at.%) by controlling the plating conditions used (tungstate concentration, glycine concentration, and current density).
3. The surface morphology of the Ni–W–B plated film was relatively smooth regardless of the film composition.
4. The grain size decreased with increasing W and B contents in the Ni–W–B film and the film with Ni content less than ca. 80 at.% was an amorphous phase.
5. The hardness of the Ni–W–B film increased with refinement of grain size up to 2–3 nm.
6. A high hardness of 800–850 Hv was demonstrated in $Ni_{82-86}W_{4-8}B_{8-12}$ (at.%) films which is comparable to that of hard chromium plated films.

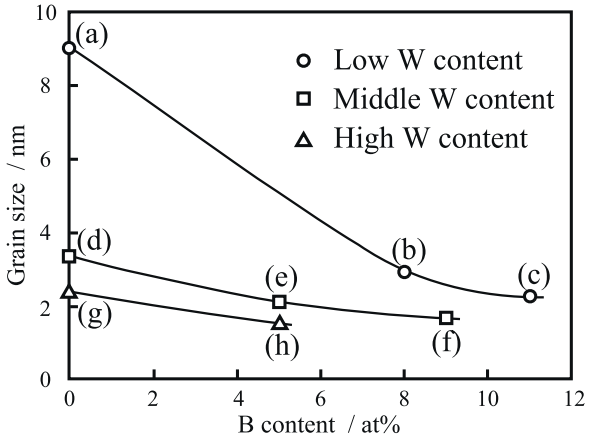

Fig. 8. Relationship between B content and grain size of ternary Ni–W–B alloy films.

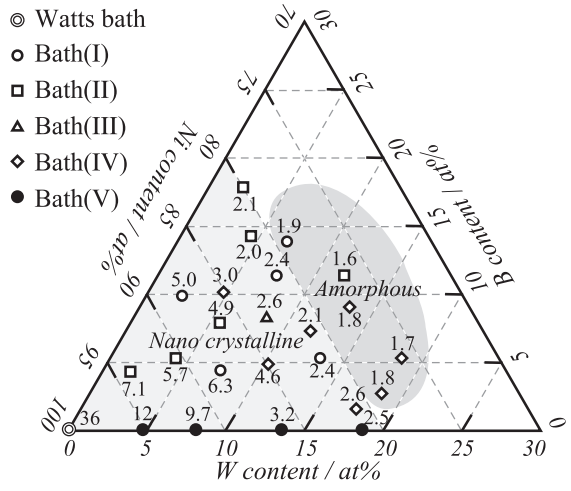

Fig. 9. Relationship between grain size and composition of ternary Ni–W–B alloy films.

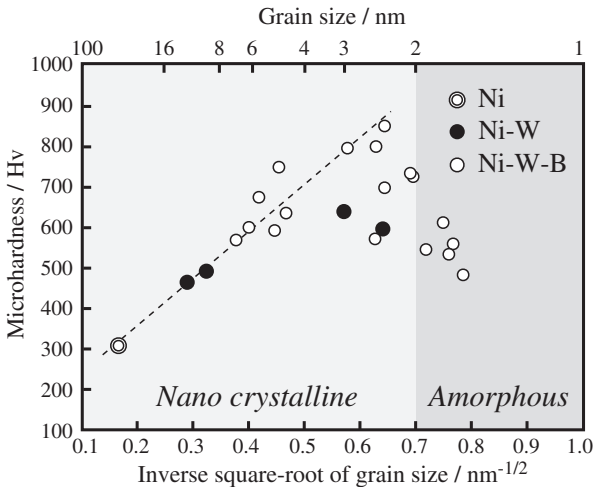

Fig. 10. Microhardness of the Ni–W–B films as a function of grain size.

Conflict of interest

There is no conflict of interest.

References

[1] C.P. Steffani, J.W. Dini, J.R. Groza, A. Palazoglu, J. Mater. Eng. Perform. 6 (1997) 413–416.
[2] L. Zhu, Q. Zhong, J. Liu, Plat. Surf. Finish. 87 (2000) 74–77.
[3] M.G. Hosseini, M. Abdolmaleki, S.A. Seyed Sadjadi, M. Raghibi Boroujeni, M.R. Arshadi, H. Khoshvaght, Surf. Eng. 25 (2009) 382–388.
[4] M.G. Hosseini, M. Abdolmaleki, S.A. Seyed Sadjadi, Prot. Met. Phys. Chem. Surf. 46 (2010) 117–122.
[5] M.G. Hosseini, M. Abdolmaleki, H. Ebrahimzadeh, S.A. Seyed Sadjadi, Int. J. Electrochem. Sci. 6 (2011) 1189–1205.
[6] G.M. Cao, F.Z. Yang, L. Huang, Z.J. Niu, S.K. Xu, S.M. Zhou, Trans. IMF 79 (2001) 81–84.
[7] F.Z. Yang, Z.H. Ma, L. Huang, S.K. Xu, S.M. Zhou, Chin. J. Chem. 24 (2006) 114–118.
[8] J. Wang, R. Xu, Y. Zhang, J. Rare Earths 30 (2012) 43–47.
[9] N. Isaev, J.G. Osteryoung, J. Appl. Electrochem. 25 (1995) 1091–1097.
[10] R.A.C. Santana, S. Prasad, A.R.N. Campos, F.O. Araújo, G.P. da Silva, P. de Lima-Neto, J. Appl. Electrochem. 36 (2006) 105–113.
[11] G. Graef, K. Anderson, J. Groza, A. Palazoglu, Mater. Sci. Eng. B 41 (1996) 253–257.
[12] G.A. Croopnick, D.M. Scruggs, Met. Finish. 92 (1994) 13–16.
[13] Y. Wu, D.-Y. Chang, S.-C. Kwon, D. Kim, Plat. Surf. Finish. 90 (2003) 46–49.
[14] O. Younes, E. Gileadi, J. Electrochem. Soc. 149 (2002) C100–C111.
[15] I. Mizushima, P.T. Tang, H.N. Hansen, M.A.J. Somers, Electrochim. Acta 51 (2005) 888–896.
[16] I. Mizushima, P.T. Tang, M.A.J. Somers, Surf. Coat. Technol. 202 (2008) 3341–3345.
[17] R. Juškėnas, I. Valsiūnas, V. Pakštas, A. Selskis, V. Jasulaitienė, V. Karpavičienė, V. Kapočius, Appl. Surf. Sci. 253 (2006) 1435–1442.
[18] T. Yamasaki, P. Schlo®macher, K. Ehrlich, Y. Ogino, Nanostruct. Mater. 10 (1998) 375–388.
[19] O. Younes, L. Zhu, Y. Rosenberg, Y. Shacham-Diamand, E. Gileadi, Langmuir 17 (2001) 8270–8275.
[20] K. Itoh, F. Wang, T. Watanabe, J. Jpn. Inst. Met. 65 (2001) 1023–1028.
[21] M. Onoda, T. Tsuchiya, K. Ogawa, T. Watanabe, J. Surf. Finish. Soc. Jpn. 41 (1990) 388–391.
[22] K.H. Lee, D. Chang, S.C. Kwon, Electrochim. Acta 50 (2005) 4538–4543.
[23] A. Giga, Y. Kimoto, Y. Takigawa, K. Higashi, Scripta Mater. 55 (2006) 143–146.
[24] C.A. Schuh, T.G. Nieh, H. Iwasaki, Acta Mater. 51 (2003) 431–443.
[25] C.A. Schuh, T.G. Nieh, T. Yamasaki, Scripta Mater. 46 (2002) 735–740.